A Hybrid Multiscale Approach in Cancer Modelling and Treatment Prediction

Gibin Powathil and Mark A.J. Chaplain

Abstract Cancer is a complex multiscale disease involving inter-related processes across a wide range of temporal and spatial scales. Multiscale mathematical models can help in studying cancer progression and serve as an in silico test base for comparing and optimizing various multi-modality anticancer treatment protocols. Here, we discuss one such hybrid multiscale approach, interlinking individual cell behavior with the macroscopic tissue scale. Using this technique, we study the spatio-temporal dynamics of individual cells and their interactions with the tumor microenvironment. At the intracellular level, the internal cell-cycle mechanism is modelled using a system of coupled ordinary differential equations, which determine cellular growth dynamics for each individual cell. The evolution of these individual cancer cells are modelled using a cellular automaton approach. Moreover, we have also incorporated the effects of oxygen distribution into this multiscale model as it has been shown to affect the internal cell-cycle dynamics of the cancer cells. The hybrid multiscale model is then used to study the effects of cell-cycle-specific chemotherapeutic drugs, alone and in combination with radiotherapy, with a long-term goal of predicting an optimal multimodality treatment plan for individual patients.

Keywords Cancer • Hybrid multiscale model • Cell cycle • Hypoxia • Chemotherapy • Radiotherapy

1 Introduction

Cancer has been and still is one of the most devastating diseases known to the developed world. Even with numerous technological, medical and pharmaceutical developments in detecting and treating different types of cancer, the median survival rates of most types of cancer remain unchanged for the last 20–30 years. One way to

G. Powathil • M.A.J. Chaplain (✉)
Division of Mathematics, University of Dundee,
Dundee, Scotland, DD1 4HN, UK
e-mail: gibin@maths.dundee.ac.uk; chaplain@maths.dundee.ac.uk

A. d'Onofrio, A. Gandolfi (eds.), *Mathematical Oncology 2013*,
Modeling and Simulation in Science, Engineering and Technology,
DOI 10.1007/978-1-4939-0458-7_8

improve this situation is to increase the survival chances of cancer patients through the intelligent planning and optimum delivery of multimodality therapies.

The most common treatments for cancer management are surgery, chemotherapy, radiation therapy and their various combinations. Chemotherapeutic drugs function by killing the cancer cells through interfering with the cell-cycle mechanism, which regulates complex intracellular processes such as proliferation, cell division and DNA replication [66]. The cell-cycle mechanism is very much dynamic in nature and is influenced by numerous intracellular pathways, extracellular interactions and the tumor microenvironment, in particular oxygen [10, 66]. Two important pathways out of many that affect the regulation of the cell cycle are the HIF-1 pathway, which is upregulated by the presence of hypoxia, and the wee1 pathway, which is influenced by circadian rhythms [37, 38]. These intracellular and extracellular heterogeneities as well as dynamical changes in the tissue microenvironment directly or indirectly contribute towards cell-cycle-mediated drug resistance and poor treatment outcome [10]. An effective way to address this is by using an appropriate combination of cell-cycle-specific chemotherapeutic drugs that targets a cancer cell at its various phases of cell division.

In most cases, chemotherapy is administered in combination with the radiation therapy, although in some cases either one of them is given alone. Just as with chemotherapy, cell-cycle dynamics also play a vital role in mediating a cell's sensitivity towards radiation therapy since the cell-cycle phase determines the cell's relative radiosensitivity [42, 53]. Previous studies have shown that cells that are in G2-M phase are more sensitive to the radiation than those in G1 phase [53]. Moreover, irradiation can also alter a cell's cell-cycle dynamics through the activation of various intracellular pathways and thus can delay the rate of progression of a cell's cell cycle, causing a group of cancer cells to accumulate in a particular phase of the cell cycle [42, 53]. The treatment-dependent perturbations of cell-cycle dynamics together with cell-cycle-dependent therapeutic sensitivity are one of many rationales behind the combination treatment protocols of chemotherapy and radiation therapy [25, 33, 53].

Clinically driven mathematical models can be used as powerful tools to understand, study, and provide useful predictions related to the outcome of various treatment protocols used to treat human malignancies. The multiscale complexity of cancer progression warrants a multiscale modelling approach to produce truly predictive mathematical models. In order to capture all the dynamics of tumor progression, we need to couple processes that are occurring at various spatial and temporal scales. In this chapter, we discuss one such hybrid multiscale model that incorporates some of the relevant intracellular, cellular and macroscopic dynamics.

2 Multiscale Mathematical Model: Growth and Progression

We consider a hybrid cellular automaton model for cancer growth and progression, which models the spatio-temporal dynamics at the cell level, interlinking cell-level dynamics to the molecular variations of intercellular signalling and macroscopic

behavior of tissue oxygen dynamics [57]. The evolution of cancer cells is modelled using a cellular automaton (CA) model where each cell has its own cell-cycle dynamics incorporated using a set of ordinary differential equations. The cells are located spatially in a dynamic microenvironment due to the variations in oxygen concentration, and the changes in oxygen distribution and drug concentration are modelled using partial differential equations. A cell-based model is considered to study the multiple effects of radiation therapy [56]. Finally, this hybrid multiscale CA modelling approach is used to analyze and study the therapeutic outcome when chemotherapy and radiation therapy are given alone and in combination with each other.

The computational simulations are performed on a two-dimensional spatial grid, where each grid represents either a cancer cell, the cross section of a blood vessel or the extracellular matrix. The spatial size of this computational grid has been chosen to approximately match the size of a single cell. To simulate the spatio-temporal progression of the cancer cells and their response to chemotherapeutic drugs and radiation, each automaton cell is associated with four major components – cells, the local oxygen (and hence HIF-1 α) concentration, initial blood vessel distribution and drug concentrations. A schematic overview of the model with the scales involved is given in Fig. 1 [56].

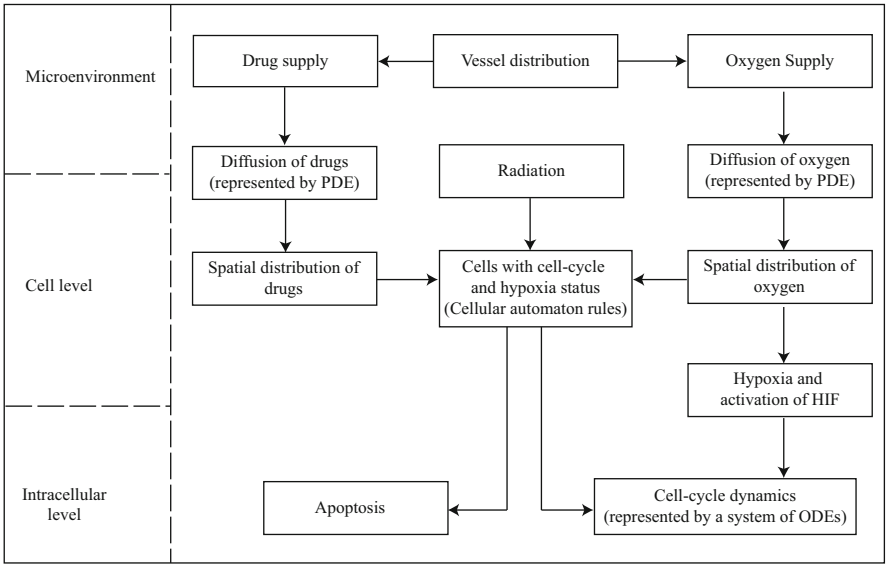

Fig. 1 Schematic diagram of the model showing the appropriate scales involved. Adapted from [56]

2.1 Intracellular Dynamics: Cell-Cycle Model

There are many different models of the cell-cycle dynamics incorporating varying underlying complexities, and details of these can be found in the key papers [7, 26, 30, 48, 74]. For our multiscale model, to model the cell-cycle dynamics within each cell, we use a simple model which was originally developed by Tyson and Novak [47, 74] that includes various relevant interactions for cell-cycle regulation and control. Using these kinetic relations, Tyson and Novak [47, 74] explain the transitions between two main steady states, G1 and S-G2-M, of the cell cycle through the changes in cell mass. Although, we use this simple model in our simulations, one could easily replace this with more complex models that describe the further complicated processes involved in the mammalian cell cycle [48].

To make the current six-variable model more relevant to the mammalian cell, we have used the equivalent mammalian proteins stated in Tyson and Novak's paper, namely the Cdk-cyclin B complex [CycB], the APC-Cdh1 complex [Cdh1], the active form of the p55cdc-APC complex [p55cdc$_A$], the total p55cdc-APC complex [p55cdc$_T$], the active form of Plk1 protein [Plk1] and the mass of the cell [mass] [57]. Following Tyson and Novak's model, the evolution of the concentrations of these components is modelled using the following system of six ODEs:

$$\frac{d[\text{CycB}]}{dt} = k_1 - (k_2^{'} + k_2^{''}[\text{Cdh1}])[\text{CycB}], \tag{1}$$

$$\frac{d[\text{Cdh1}]}{dt} = \frac{(k_3^{'} + k_3^{''}\,[\text{p55cdc}_\text{A}])(1 - [\text{Cdh1}])}{J_3 + 1 - [\text{Cdh1}]} - \frac{k_4[\text{mass}][\text{CycB}][\text{Cdh1}]}{J_4 + [\text{Cdh1}]}, \tag{2}$$

$$\frac{d\,[\text{p55cdc}_\text{T}]}{dt} = k_5^{'} + k_5^{''}\frac{([\text{CycB}][\text{mass}])^n}{J_5^n + ([\text{CycB}][\text{mass}])^n} - k_6\,[\text{p55cdc}_\text{T}], \tag{3}$$

$$\frac{d\,[\text{p55cdc}_\text{A}]}{dt} = \frac{k_7[\text{Plk1}](\,[\text{p55cdc}_\text{T}] - \,[\text{p55cdc}_\text{A}])}{J_7 + \,[\text{p55cdc}_\text{T}] - \,[\text{p55cdc}_\text{A}]} - \frac{k_8[Mad]\,[\text{p55cdc}_\text{A}]}{J_8 + \,[\text{p55cdc}_\text{A}]} - k_6\,[\text{p55cdc}_\text{A}], \tag{4}$$

$$\frac{d[\text{Plk1}]}{dt} = k_9[\text{mass}][\text{CycB}](1\text{-}[\text{Plk1}]) - k_{10}[\text{Plk1}], \tag{5}$$

$$\frac{d[\text{mass}]}{dt} = \mu[\text{mass}]\left(1 - \frac{[\text{mass}]}{m_*}\right), \tag{6}$$

where k_i are the rate constants and the values are chosen in proportional to those in Tyson and Novak so that the time scale is relevant to mammalian cell cycle [47, 74].

Here, the equation governing the change of mass accounts for the growth of each cell. A cell is assumed to divide when the concentration of Cdk-cyclin B complex [CycB] crosses a specific threshold value $[\text{CycB}]_{th}$ which is assumed to be 0.1, from above and then the mass, [mass] is halved. To introduce a random growth rate for

individual cells which in turn introduces cell-cycle heterogeneity in the population, we consider a varying growth rate μ:

$$\mu = \mu^{+} + \varepsilon\hat{\mu}, \tag{7}$$

where $\mu^{+} = 0.03$, $\varepsilon = 0.006$ and $\hat{\mu}$ is a probability density function with uniform distribution between -1 and 1. The rest of the parameter values of the cell-cycle model can be found in Powathil et al. [57].

Figure 2 shows the changes in various protein concentrations that have been included in the current cell-cycle model for one single automaton cell. Every cell in this multiscale model has similar cell-cycle dynamics built-in which further control the division and cell-cycle phases of the respective cells. In this representative figure (Fig. 2), a cell undergoes division constantly as long as there is enough space to divide and the surrounding microenvironment is favorable for its division. However, as soon as its neighboring spaces are occupied, the cell moves to a resting phase where the concentrations are maintained in a constant level and in Fig. 2, this happens at around 190 h.

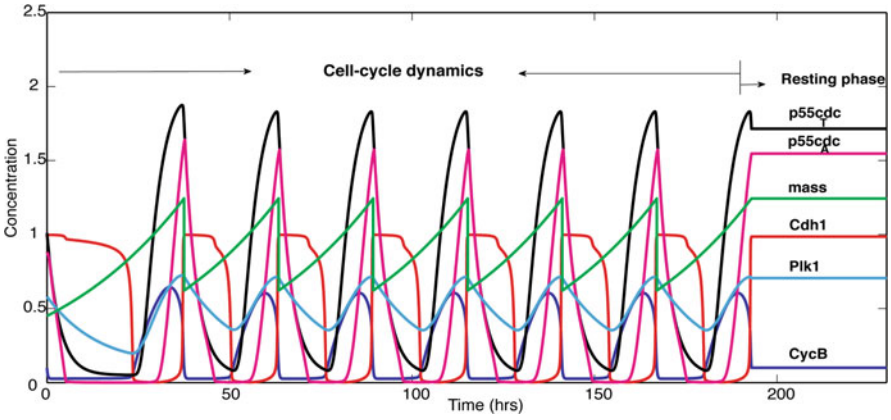

Fig. 2 Plot of the concentration profiles of the various intracellular proteins and the cell mass over a period of 200 h for one automaton cell in the model. This is obtained by solving the system of equations, Equations 1 to 6, with the relevant parameter values from Table 1. Adapted from [57]

Table 1 cell-cycle model parameters from [55]

Component	Rate constants (hr^{-1})	Dimensionless constants
[CycB]	$k_1 = 0.12$, $k_2' = 0.12$, $k_2'' = 4.5$, [p27/p21]=1.05	$[\text{CycB}]_{th} = 0.1$
[Cdh1]	$k_3' = 3$,$k_3'' = 30$, $k_4 = 105$	$J_3 = 0.04$,$J_4 = 0.04$
[p55cdc$_\text{T}$]	$k_5' = 0.015$, $k_5'' = 0.6$, $k_6 = 0.3$	$J_5 = 0.3$, $n = 4$
[p55cdc$_\text{A}$]	$k_7 = 3$,$k_8 = 1.5$	$J_7 = 0.001$,$J_8 = 0.001$,[Mad]=1
[Plk1]	$k_9 = 0.3$, $k_{10} = 0.06$	
[mass]	$\mu^{+} = 0.03$	$m_* = 10$

2.2 Macroscopic Effects: Oxygen Dynamics and Hypoxia

At the macroscopic level, the effects of the changing tissue microenvironment are incorporated into the model by introducing oxygen dynamics which are modelled using a suitable partial differential equation incorporating vessels as sources of oxygen. Computationally, there are several ways of introducing vascular dynamics into the model depending on various temporal and spatial scales of interest [9, 15, 67]. Here, we have considered blood vessel cross sections distributed randomly throughout the two-dimensional domain with density $\phi_d = N_v/N^2$, where N_v is the number of vessel cross sections [18,36]. If $K(x,t)$ denotes the oxygen concentration at position x at time t, then its spatio-temporal evolution can be expressed as,

$$\frac{\partial K(x,t)}{\partial t} = \nabla.(D_K(x)\nabla K(x,t)) + r(x)m(x) - \phi K(x,t)\text{cell}(x,t), \tag{8}$$

where $D_K(x)$ is the diffusion coefficient and ϕ is the rate of oxygen consumption by a cell at position x at time t ($\text{cell}(x,t) = 1$ if position x is occupied by a cancer cell at time t and zero otherwise). Here, $m(x)$ denotes the vessel cross section at position x ($m(x) = 1$ for the presence of blood vessel at position x, and zero otherwise); thus the term $r(x)m(x)$ describes the production of oxygen at rate $r(x)$ [57]. The diffusion coefficient and the supply rate of the oxygen vary depending on the location of the cancer cells and blood vessels [57]. Since it has been observed that when a vessel is surrounded by a mass of densely packed cancer cells its perfusion and diffusion capabilities are seriously impaired, this is incorporated in our model by considering a lower diffusion rate and a lower supply rate in the tumor as compared to the normal vessels [57]. This equation is solved using no-flux boundary conditions and an appropriate initial condition [55]. Figure 3 shows a representative profile of the spatial distribution of oxygen concentration after solving Equation (8) with relevant parameters as given below.

The oxygen diffusion length scale L can be considered to be approximately equal to 100 μm and the value of the diffusion constant is taken as $2 * 10^{-5}$ cm^2/s [50]. Using these and the relation $L = \sqrt{D/\phi}$, the mean oxygen uptake can be approximately estimated as 0.2 s^{-1}. The oxygen supply through the blood vessel is approximately taken as $8.2 * 10^{-3}$mols s^{-1} [44]. The appropriate nondimensionalization will yield a time scale of $T = 0.001$hr and hence each time step is set to be 0.001hr for both CA time step and oxygen dynamics. The length scale of 100μm will give a square grid of length $\Delta x * L$=20 μm, approximate diameter of a cell and thus a tumor of radius 1 mm [57].

The changes in the oxygen concentration, especially hypoxia, may affect various intra and intercellular processes of the cells that constitute the tumor mass. In the present model, the effects of hypoxia are included through the activation and inactivation of HIF-1 α which further results in changes in intracellular cell-cycle dynamics. When oxygen concentration at a specific position x falls below 10% (hypoxic cell), HIF-1α is assumed to become active from an inactive phase, which

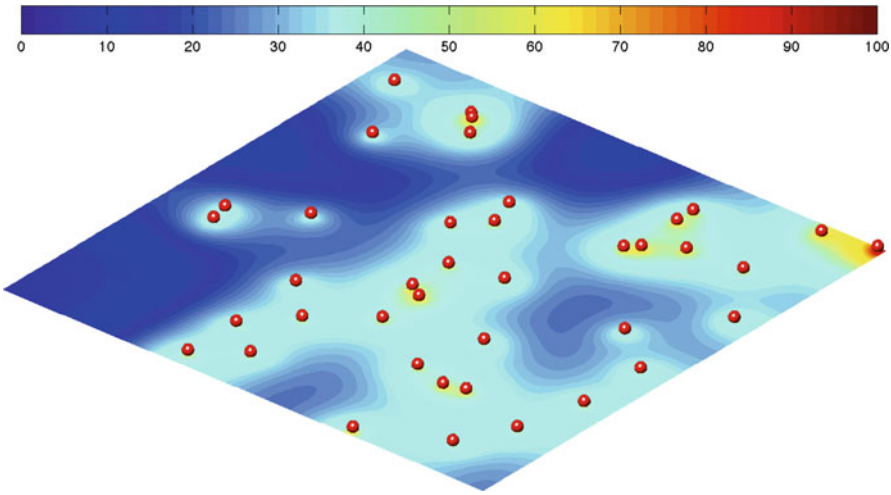

Fig. 3 Plot showing the concentration profile of oxygen supplied from the vasculature. The *red-colored spheres* represent the blood vessel cross sections and the color map shows the percentage of oxygen concentration. Adapted from [56]

further delays the cell-cycle dynamics through the upregulation of p27/p21 pathway [29, 57]. This is incorporated into Equation (1) using an additional decay term proportional to the concentration of p27/p21 (which is considered here as constant) [4, 57]. Thus the modified equation for cyclic-CDK dynamics can be written as

$$\frac{d[\text{CycB}]}{dt} = k_1 - (k_2^{'} + k_2^{''}[\text{Cdh1}] + [\text{p27/p21}][HIF])[\text{CycB}], \tag{9}$$

where

$$[HIF] = \begin{cases} 1: & K(x,t) \leq 10\% \\ 0: & K(x,t) > 10\%. \end{cases} \tag{10}$$

2.3 Cancer Growth and Progression: Cellular Automaton Model

Here, we use a cellular automaton (CA) approach to study the spatial and temporal dynamics at the cell level incorporating the intracellular and macroscopic details described above. Previously, cellular automaton modelling approaches have been used to model various aspects of tumor development and progression, including the formation of multicellular spheroids [35, 52], tumor-induced angiogenesis [9], cancer cell adhesion and invasion [73]. Moreover, several hybrid CA models have

already seen use to study tumor growth and development in multiple scales and time [3, 5, 21, 28, 49, 52, 54, 60].

Here, the computational model is simulated on a spatial grid of size 100×100 grid points and each automaton element whether it is empty or occupied has a physical size of $l \times l$, where $l = 20\ \mu m$, simulating a cancer tissue of $2 \times 2\ mm^2$ area. The CA begins as a new grid of empty points with a single initial cell in G1 phase (blue cell) of the cell cycle at the center. This initial cell divides following the intracellular cell-cycle dynamics modelled using Equation 1–6 and produces a cluster of cells on a regular square lattice with no-flux boundary conditions. The PDE equation governing the oxygen dynamics is simulated using a finite difference scheme and the system of ordinary differential equations controlling cell-cycle dynamics is solved using the Runge-Kutta method to obtain the intracellular protein concentrations for each cell. At each simulation step, these intracellular protein levels are checked for each individual cell and its cell-cycle phase is updated accordingly. A cell is considered to be in S-G2-M phase (green cell) if its [CycB] level is greater than a specific threshold and if it is lower than this value, the cell is in G1 phase. If the cyclin B-cdk complex concentration [CycB] crosses this threshold from above, the cell is considered ready for division. Once the cell is marked for division, its neighborhood of order 3 is checked for an empty space with highest oxygen gradient and the cell undergoes cell division and its mass [mass] is halved. If the cell's neighborhood has "no space" then its growth rate μ is set to zero and it enters a resting state (magenta cell). After the division, the new cell is placed with a G1 state of cell cycle and is assigned a value for μ randomly from the range of values of μ. If there are more than one empty space with same oxygen gradient, a position is chosen randomly. The position of the new daughter cells is determined by Moore and von Neumann neighborhood alternatively to avoid the associated cell distribution patterns specific to each method [56, 57].

As this multiscale model evolves over time, the number of cells increases and the oxygen consumption also increases accordingly, eventually leading to tissue hypoxia. Here, the hypoxic cells that are in G1 phase are represented by rose color-coded cells while hypoxic S-G2-M cells and hypoxic resting cells are denoted by the colors yellow and silver, respectively. Figure 4 shows a snapshot of the multiscale hybrid CA model after 700 h where Fig. 4a illustrates the distribution of oxygen in a percentage scale, Figure 4(b) gives the HIF-1α map and Fig. 4c shows the distribution of cells in various cell cycle phases. Proliferating cells which are active in cell-cycle are mainly seen near the high oxygen concentration regions of the tumor boundary, creating fingerlike growth pattern in the tumor cell distribution. This is mainly due the to effect of surrounding microenvironment as the tumor tends to advance towards the most favorable microenvironment that supports its growth and invasion. In Fig. 5 we plot the corresponding total number of cells along with the number of cells in each of the various cell-cycle phases against time for this asynchronous population.

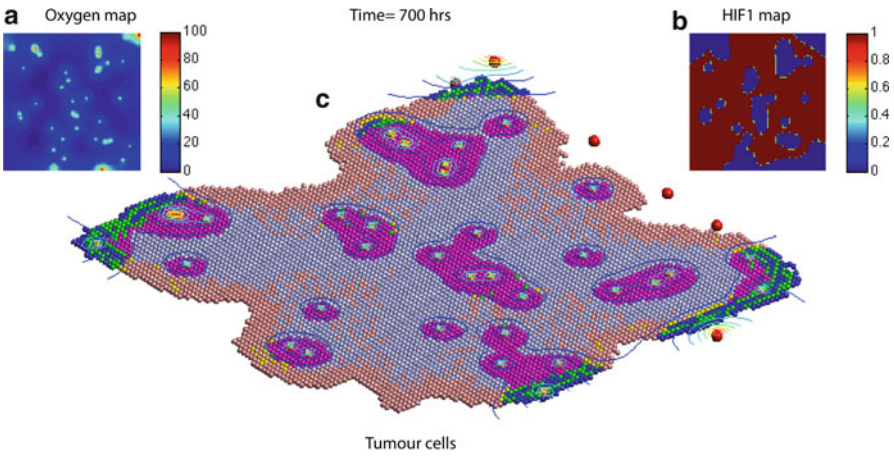

Fig. 4 Plots showing a snapshot of the simulation results of the model at time= 700 h. (**a**) plot of the oxygen concentration distribution within the spatial domain, (**b**) plot of the HIF-1 α concentration within the spatial domain and (**c**) plot of the spatial distribution of the cells in different stages of the cell cycle which are G1 (*blue*), S-G2-M (*green*), resting (*magenta*), hypoxic cells in G1 (*rose*), hypoxic cells in S-G2-M (*yellow*) and hypoxic cells in resting (*silver*). The contours represent the oxygen concentration profiles. Adapted from [57]

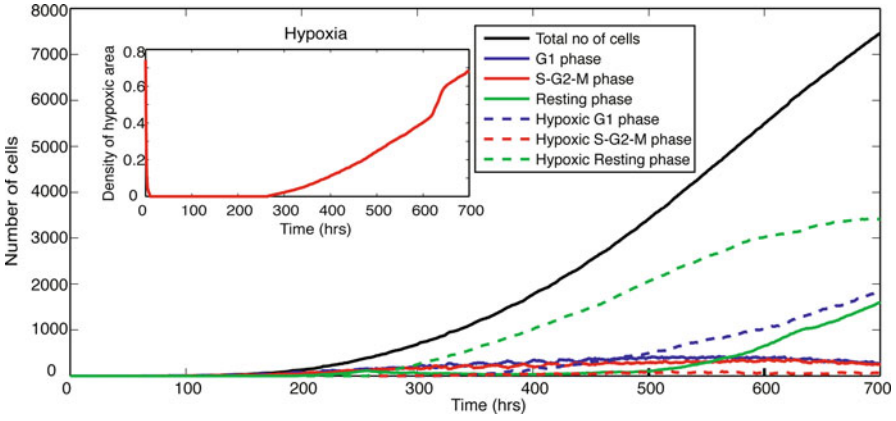

Fig. 5 Plot showing the total number of cells in the different phases of the cell cycle over the course of one simulation run representing 700 h. The subplot shows the density of hypoxic area as a function of time. Adapted from [57]

3 Mathematical Model: Effects of Anticancer Treatments

Chemotherapy and radiotherapy play important roles in the primary treatment of many cancers and in improving the survival after cancer surgery. Currently, numerous chemotherapeutic drugs and irradiation techniques are employed, which

have evolved over several decades through empirical clinical usage. The effectiveness of these treatment protocols is also considerably affected by internal tumor heterogeneities caused by perturbations in the intracellular pathways as well as by the dynamical changes in the tissue microenvironment, in particular oxygen concentration [10]. Hence, it is also important to consider such heterogeneity when studying various optimization protocols, as this can help in improving the delivery of multi-modality treatments. Mathematical modelling of such complex dynamic situations might provide one solution to this problem, and speed up the delivery of efficacious treatments to patients while preventing the use of potentially sub-optimal treatment combinations. Mathematical and computational models can also be very helpful in gaining valuable insights into the mechanisms and consequences of various complex intra-cellular and intercellular changes during and after the therapy. Here, we use the hybrid multiscale cellular automaton model described previously, incorporating the effects of oxygen heterogeneity and cell-cycle dynamics to study the multiple effects of cell-cycle-dependent chemotherapy and radiotherapy.

3.1 Modelling the Effects of Cell-Cycle-Specific Chemotherapy

Several previous mathematical models have shed light on understanding the effects of chemotherapy and its optimal delivery [1, 17, 60, 68]. Chemotherapy is a commonly used treatment for cancer. Chemotherapeutic drugs act on rapidly proliferating cells, such as cancer cells, by interfering with the cell-cycle and other cell-cycle specific targets. Cell-cycle-specific anticancer drugs are more effective on dividing cells by interfering with the cell-cycle and other cell-cycle-specific targets. Hence, it might be more efficient to use a combination of multiple cell-cycle phase-specific drugs that target the cells in different phases of the cell cycle. Here, the concentration of chemotherapeutic drug type i, $C_i(x,t)$ is governed by a similar equation as that of oxygen distribution (8), given by;

$$\frac{\partial C_i(x,t)}{\partial t} = \nabla.(D_{ci}(x)\nabla C_i(x,t)) + r_{ci}(x)m(x) - \phi_{ci}C_i(x,t)\text{cell}(x,t) - \eta_{ci}C_i(x,t), \tag{11}$$

where $D_{ci}(x)$ is the diffusion coefficient of the drug, ϕ_{ci} is the rate by which the drug is taken in by a cell (assumed to be zero as it is very negligible when compared to oxygen uptake), r_{ci} is the drug supply rate by the pre-existing vascular network and η_{ci} is the drug decay rate [55].

Drug molecules are much bigger in size than oxygen molecules and their supply through the normal blood vessels is minimal. Additionally, the drug diffusion rate varies depending on the vessel location within the domain and with other factors such as pressure. Hence, similar to our assumptions for oxygen, these effects of pressure are taken into account through the following assumptions related to the

transport properties and delivery rate of the drug [57]. The parameters that are used in the equations governing the dynamics of chemotherapy are chosen in comparison with oxygen molecules and other known compounds of similar molecular mass [57]. In the model, chemotherapeutic drugs are assumed to be effective in killing a cell with a probability p_i, if its concentration at that location of the cell is above a fixed threshold value θ_{ci} and below which the drug has no effect on any cells. Using this model, we have further analyzed the effects of these drugs which are delivered at a same rate in two different combinations targeting either the same phase or a different phase of the cell-cycle.

The temporal evolution of the tumor dynamics when the time delay between two drug doses is 84 h (chosen as a representative illustration) is given in Figs. 6, 7 and 8. Figs. 6a–d and 7a–d show the changes in the total number of cells as well as the number of cells that are in various phases of the cell-cycle when the phase-specific drugs are delivered in multiple combinations. Figure 8 illustrates the spatial evolution of the cancer cell distribution during the administration of the chemotherapeutic drugs. These dynamical changes in the spatial evolution of cancer cell distribution will have a significant impact on the final cell distribution when more than two doses of cell-cycle-specific chemotherapy are administered subsequently. Hence, it is very important to consider the cell-cycle heterogeneity together with the oxygen heterogeneity while studying the effects of these drugs to obtain an accurate prediction.

The graph in Fig. 6a shows that when the delay is 84 h, the combination of two S-G2-M state-specific drugs gives a slightly better cell kill at the final simulation time as compared to the other three possible combinations of these two drug doses. The worst combination is the delivery of two G1-specific drug doses while other two combinations give a similar outcome as that of the application of two S-G2-M drugs. This can be explained by the presence of internal heterogeneity due to the cell-cycle dynamics which oscillates between the G1 and S-G2-M states. When the first dose is given, the majority of the cells that are in the vicinity of the diffused drug concentration might happen to be in the G1 state, leaving the cells in the other cycling phase, hence synchronizing the cell population. When a fraction of the cells is killed by the delivered drug, the remaining cells undergo a spatial redistribution that further changes the dynamics of oxygen and drug concentrations, which will eventually affect the future drug delivery. Interestingly, although the first or second doses of G1-specific drug kill more cells than that of S-G2-M-phase drug, some combination involving a G1-phase drug results in a higher number of surviving cells at the final time, 700 h. This is because the higher rate of cell kill eliminates most of the cells in the resting phase, increasing the number of available free space and decreasing the hypoxic area (Figs. 7, 8). As free space is created by the cell kill, the resting cells will return to their active cell cycle and these viable cells utilize this favorable microenvironment to proliferate rapidly and reach a maximum size in the absence of further doses of chemotherapy. An extensive analysis and results are given in [57].

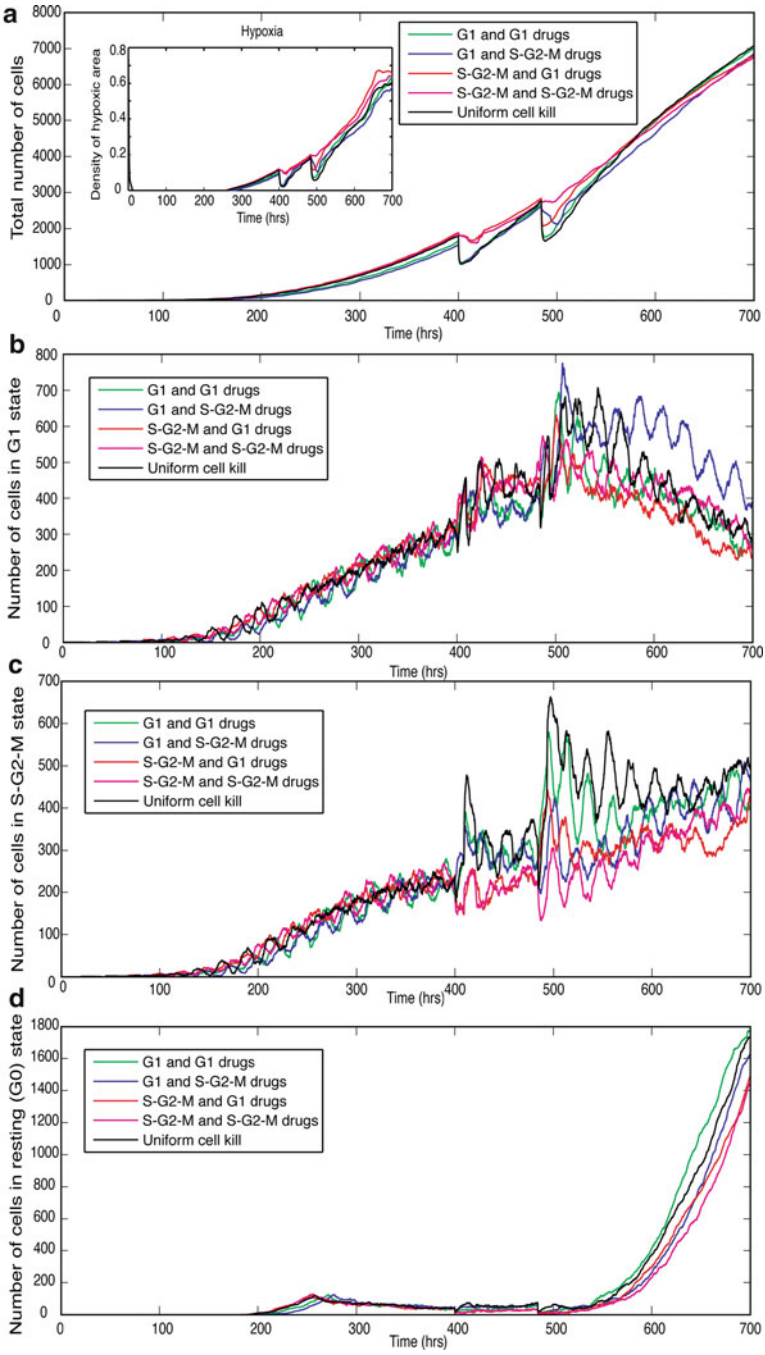

Fig. 6 Plots showing the total number of cells as well as the number of cells in different states as a function of time when two drug doses are given with a time delay of 84 h. (**a**) plot showing the total number of cells and subplot showing the density of hypoxic area over time, (**b**) Plot showing the number of cells in G1 state, (**c**) plot showing the number of cells in S-G2-M state and (**d**) Plot showing the number of cells in G0 state. Adapted from [57]

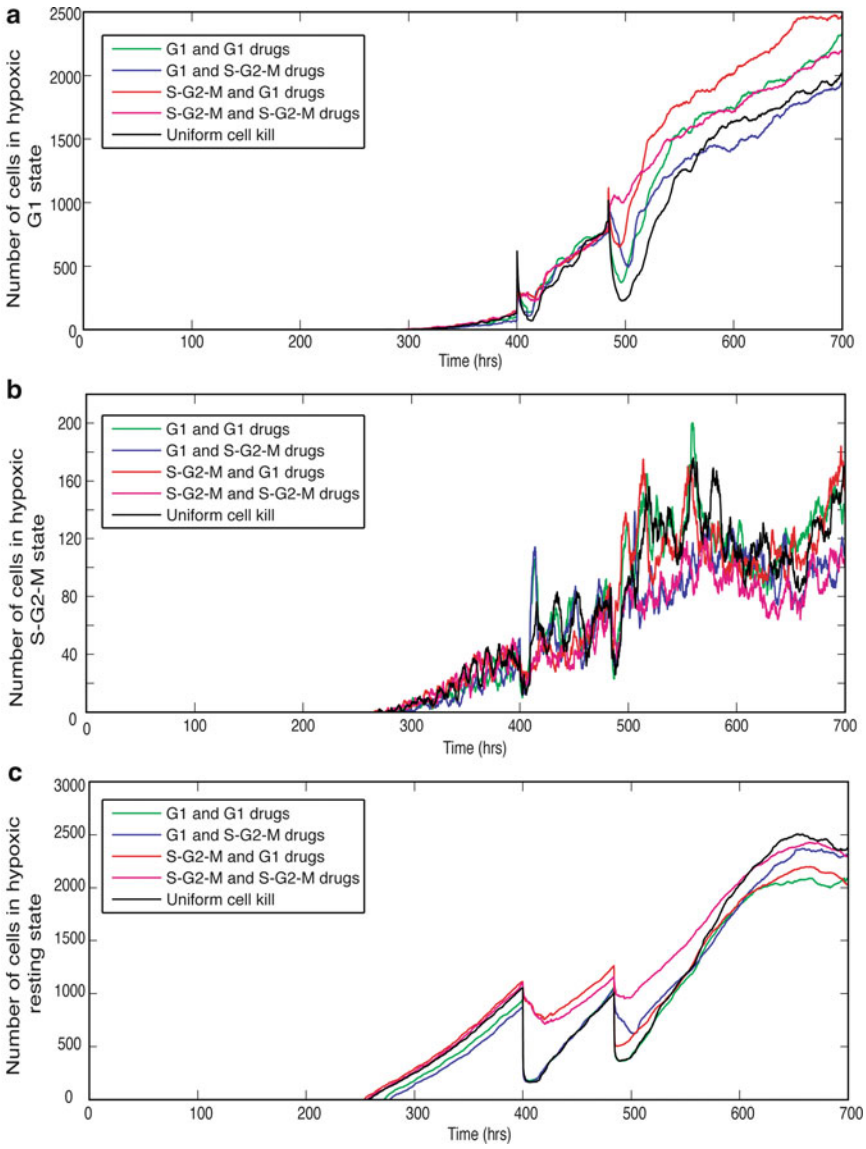

Fig. 7 Plots showing the number of cells in different states as a function of time when two drug doses are given with a time delay of 84 h. (**a**) Plot showing the number of cells in G1 state that are in hypoxic region, (**b**) plot showing the number of cells in S-G2-M state that are in hypoxic region and (**d**) plot showing the number of cells in G0 state that are in hypoxic region. Adapted from [57]

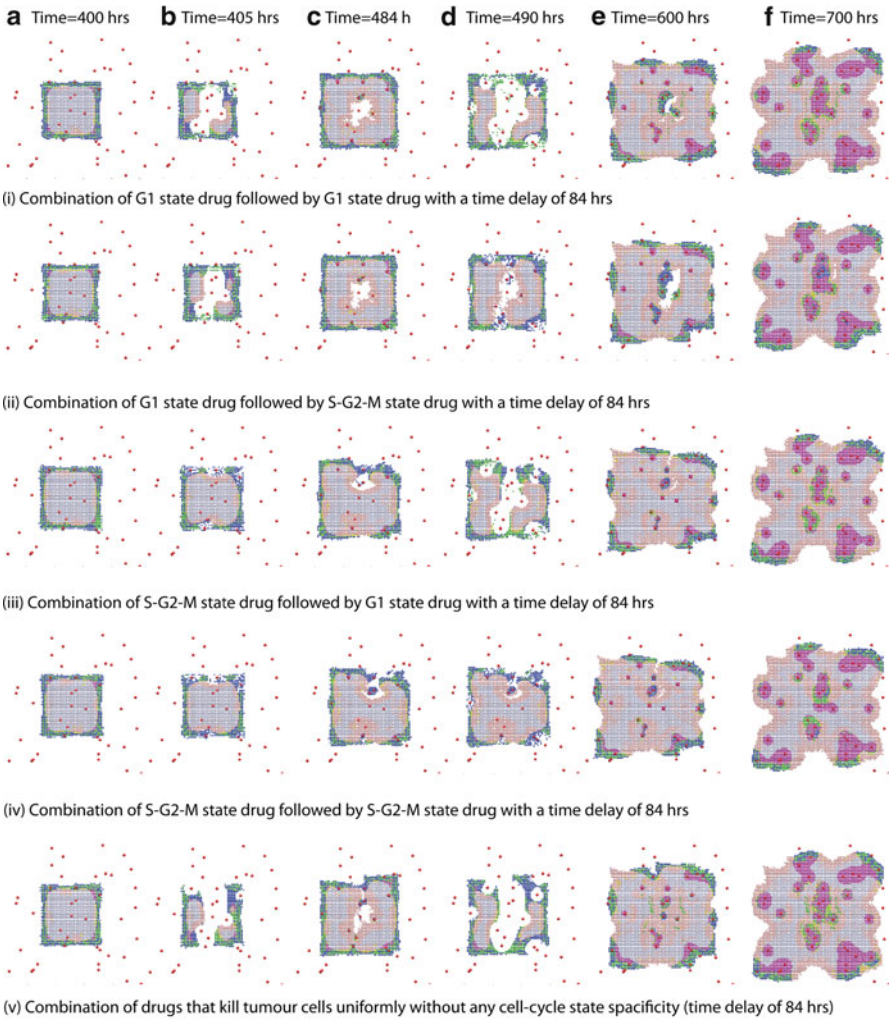

Fig. 8 Plots showing the spatial distributions of cells within a growing solid tumor at time = 400 h (delivery of 1st drug, column (**a**)), time=405 h (column (**b**)), time=484 h (2nd drug delivery, column (**c**)), time=490 h (column (**d**)), time=600 h (column (**e**)) and time=700 h (final time, column (**f**)), for various combinations of cell-cycle-specific drugs (i to v). These figures show that consideration of spatial distribution of cells may highly benefit in planning and optimizing the delivery of cell-cycle-dependent drugs. Adapted from [57]

3.2 Modelling the Effects of Radiation Therapy

In a similar manner to chemotherapy, the key intracellular processes such as cell-cycle dynamics and external factors including oxygen distribution also play a vital role in determining the radiosensitivity of cells that are irradiated [53, 71].

In addition, the delivered radiation fractions (treatments) further dynamically change this radiosensitivity over time by redistributing the cancer cells within the cell cycle by inducing repopulation of the tumor mass, by allowing reoxygenation of the tumor and by activating DNA repair mechanisms [42, 53, 71]. Traditionally, the survival fraction of cells after they are irradiated is calculated using the linear quadratic (LQ) model [65]. The LQ model considers the effects of both irreparable damage and repairable damage susceptible to misrepair. One of the basic assumptions of the LQ model is that a cell is damaged through double-strand breaks (DSBs) of its DNA, leading to reproductive cell death. This damage to DNA can happen in two different ways, which are captured in the LQ model through its linear and quadratic terms. The linear term accounts for the DSBs due to one single hit of radiation whereas the quadratic term represents the effects of two separate ionizing events that eventually cause DNA DSBs [65]. Assuming that the probability of one interaction causing a DSB is linearly proportional to the dose d, the survival fraction in the LQ model can be written as

$$S(d) = \exp(-\alpha d - \beta d^2), \tag{12}$$

where d is the radiation dose and α and β are sensitivity parameters, taken to be $\alpha = 0.3\ Gy^{-1}$ and $\beta = 0.03\ Gy^{-2}$ [55].

As discussed above, experimental observations indicate that the relative radiation sensitivity of a cancer cell depends on multiple factors, including its oxygenation status and its cell-cycle phase [6, 53, 75]. While the cells are found to be more sensitive when in the S-G2-M phase as compared with the G1 phase, their relative radiation sensitivity is minimal at low oxygen levels. The effect of changing tissue oxygen levels within the spatial domain on the radiation sensitivity can be incorporated into the LQ model (Eq. 12) by using the concepts of an oxygen enhancement ratio (OER) or oxygen modification factor (OMF) [55], defined as

$$\text{OMF} = \frac{\text{OER}(pO_2)}{\text{OER}_m} = \frac{1}{\text{OER}_m} \frac{\text{OER}_m . pO_2(x) + K_m}{pO_2(x) + K_m}, \tag{13}$$

where $pO2(x)$ is the oxygen concentration at position x, OER is the ratio of the radiation doses needed for the same cell kill under anoxic and oxic conditions, $\text{OER}_m = 3$ is the maximum ratio and $K_m = 3$ mm Hg is the $pO2$ at half the increase from 1 to OER_m [55]. Furthermore, a varying radiation sensitivity based on the cell's cell-cycle status is incorporated into the LQ model using a parameter γ, which varies from 0 to 1, depending on the individual cell's position at the time of the irradiation. Here, we assumed that the cells in S-G2-M phase have maximum sensitivity with $\gamma = 1$, while the cells in G1 phase and the resting phase have relative sensitivities of $\gamma = 0.5$ and $\gamma = 0.25$, respectively.

The equation for survival probability (LQ model, Eq. 12) is then modified by incorporating this varying sensitivity due to the changes in cell-cycle phase and oxygen levels by additional terms γ and OMF [56], as follows:

$$S(d) = \exp\left[\gamma\left(-\alpha.\mathrm{OMF}.d - \beta(\mathrm{OMF}.d)^2\right)\right]. \tag{14}$$

The effects of cellular repair are included in the model by assuming that 98% of damage caused by the radiation is likely to be repaired within few hours of radiation, if they are treated with low-dose radiation (< 5 Gy) [31, 72] and allowing the cells to stay in the same phase (divisional delay) for an extra time duration of up to 9 h for repairing the damage [42]. This survival probability is then used to calculate the survival chances of each cell when they are irradiated with the radiation rays. To study this survival chance of an individual cell, a random number is drawn for each cell at every time when it is irradiated and compared against the calculated survival probability. The irradiated cell survives if the random number is smaller than the survival probability and dies otherwise.

This single-cell-based radiation model is used to study multiple factors involving radiation therapy. To study cell-cycle dynamics when cells are treated with multiple fractions of radiation, we have simulated the radiation therapy of the cancer cells with 2.5 Gy/day for 5 days, up to 12.5 Gy starting at time = 400 h. This is compared against the results of irradiation with a single dose of 12.5 Gy given at time = 400 h and the control cell distribution. The total number of cells and the number of cells that are in G1, G2 and resting phases (b) when cells are treated with a single dose of radiation and (c) when the cells are treated with fractional doses of radiations are plotted against time in Figs. 9b and c, respectively [56]. The subplot in these Figures show the percentage of hypoxic area with respect to the time. Figure 9b shows that when the cells are irradiated with a single dose of radiation, the majority of the cells stay in G2 phase of the cell-cycle after the radiation for a short period and then the majority move into G1 and stay in that distribution for about 60–70 h (partial synchronization) before eventually recovering and following the cycling pattern seen in the case of the control cell population. However, when the total dose of 12.5 Gy is given in 5 small doses, the synchronization is observed only during the treatment time and is lost as soon as the radiation is stopped (Fig. 9c). In both cases, the number of cells in resting phase decreases as the resting cells re-enter the active phase of the cell cycle (into G1 phase) with the creation of empty spaces and a favorable microenvironment.

Figure 10 shows the analysis of various factors affecting a cell's radiation sensitivity. Figure 10a shows the temporal changes in the total number of cells and the cells that are in various phases of the cell cycle, when cells are irradiated with 2.5 Gy/day for 5 days in a 100 % oxygenated microenvironment. In Fig. 10b, we plot the number of cells if no cell-cycle delay after the radiation is assumed. The effects of radiation therapy on the number of cells when no cell-cycle specificity for the radiation sensitivity is assumed are given in Fig. 10c. The number of cells for the case where no DNA repair is assumed is plotted in Fig. 10d and shows an increase in the number of cells killed as compared to the normal case as expected.

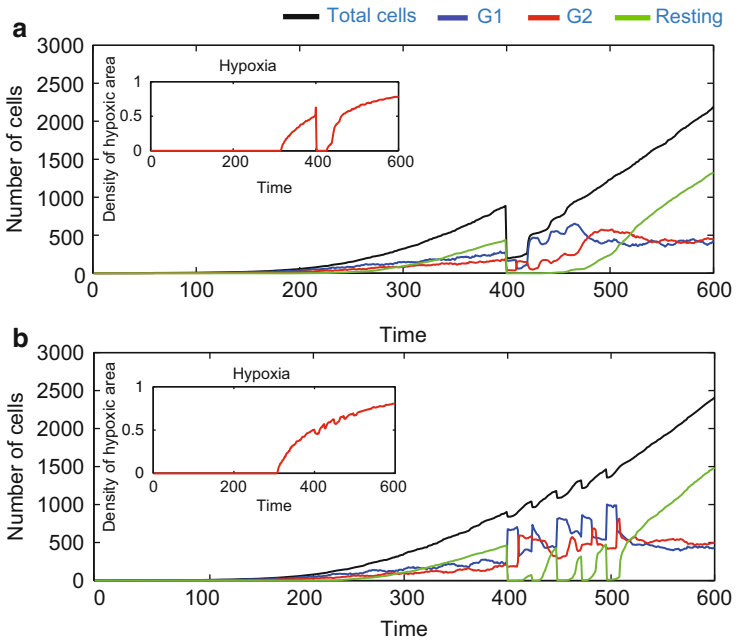

Fig. 9 Number of cells in G1, G2 and resting phases for a heterogeneous environment. The number of cells (**a**) under single dose of radiation with 12.5 Gy and (**b**) under fractional radiation starting at time =400 h (5 fractions of 2.5 Gy). Adapted from [56]

In all four cases (Fig. 10), after the irradiation, the presence of a favorable tissue microenvironment increases the number of cells in active cell cycle. It can be seen from Fig. 10 that out of four factors that we have considered, the cell-cycle phase-specific radiation sensitivity of the individual cells and the activation of the repair mechanisms within the cell significantly affect the relative radio-sensitivity of a cell.

We have also analyzed the usefulness of the developed model by comparing the simulation results of the model with the experimental results when the cells are irradiated with a radiation dose of 3 Gy. The comparison results are given in Fig. 11 [16, 56]. The results show that the controls have cells predominantly distributed in G1 as compared to G2. After irradiation, the majority of the cells started to accumulate in G2 phase, about 12 h after irradiation, and stayed in G2 phase before going back to a G1-phase-dominant cell distribution by 22–24 h after irradiation. The results show a qualitative agreement with the experimental results. More analyses about the model and additional results can be found in [56].

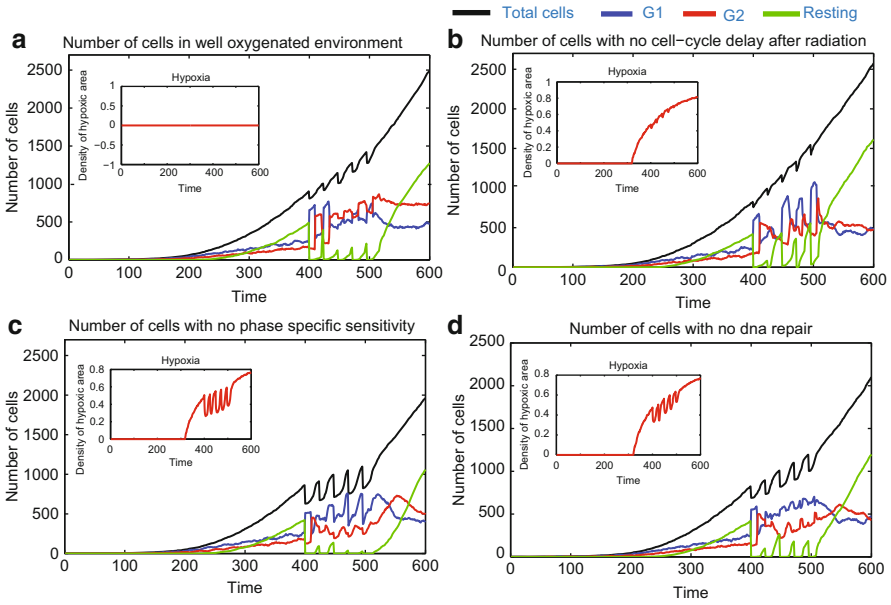

Fig. 10 Number of cells under various conditions that influence the radiation damage after the irradiation. (**a**) Plots for a well-oxygenated microenvironment, (**b**) plot assuming no cell-cycle delay for repair after the radiation, (**c**) plots assuming there is no cell-cycle phase-specific sensitivity for repair after the radiation and (**d**) plots when there is no DNA repair after the radiation. Adapted from [56]

3.3 Modelling the Effects of Combination Therapy

Clinically, a kinetically based administration of chemotherapy and radiation therapy is often observed to give a better outcome than that of chemotherapy or radiation therapy alone [25, 33, 53]. Studies have shown that both radiation therapy and chemotherapeutic drugs can induce a cell-cycle synchrony and arrest cells at a particular cell-cycle phase which improves the effectiveness of the next dose of radiation/chemotherapy [25, 53]. However, most of these interactions are dependent on the type of drugs given and their combinations among their doses and radiation fractions. Hence an appropriate combination of these therapeutic modalities is an essential requirement to achieve a maximum survival [32, 34]. Here, we use our multiscale model to study two different combination regimes of radiation therapy and chemotherapy and some of the representative results are given in Figs. 12 and 13. Note that in these combinations, we keep the total treatment time constant to compare their effects on tumor control. We have also used the same set of parameter values and doses for each phase-specific chemotherapy [57].

Figure 12 shows the effects of combination treatments when two doses of the chemotherapy drugs are given after radiation therapy at times = 466 h and 496 h.

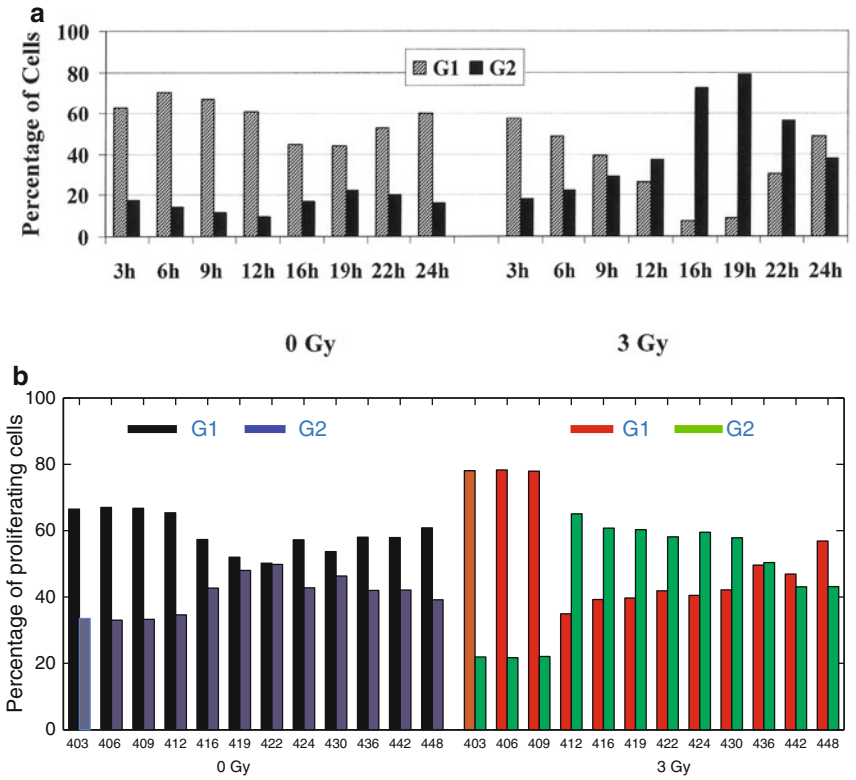

Fig. 11 Percentage of cells in G1 and G2 states with and without radiation. (**a**) Experimental results from [16]. Cells were irradiated with 3 Gy and samples were taken after 3 h, 6 h, 9 h, 12 h, 16 h, 22 h and 24 h for flow cytometry analysis. The cell-cycle distribution of irradiated cells was compared to unirradiated cells collected at the same time points. The left peak in each case represents cells in G1 and the right peek represents cells in G2 phase. From Chaudhry [16] (BioMed Central OpenAccess). and (**b**) Simulation results (percentage of proliferating cells). The percentage of proliferating cells in G1 and G2 phases when the cell is irradiated with dose=3 Gy at time=400, 403, 406, 409, 412, 416, 419, 422, 424, 430, 436, 442 and 448 h. The cell-cycle distribution of irradiated cells was compared to unirradiated cells collected at the same time points. The results show a qualitative agreement with the experimental results. Adapted from [56]

The radiation starts at time= 340 h with a fractional daily dosage of 2 Gy for 5 days. Here, the radiation given before two doses of chemotherapy introduces a partial cell-cycle synchrony of cell distribution that remains until the end of the therapy. The cell-phase distribution for the case when the doses of chemotherapeutic drug are given before and after the radiation is plotted in Fig. 13. The administration of a G1-phase-specific chemotherapeutic drug redistributes the cells so that the majority of the cells are in G1 phase throughout the radiation period. This is the consequence of an increased cell kill, that promotes an increased proliferation as cells will re-enter the active phase of the cell cycle (G1) when conditions become

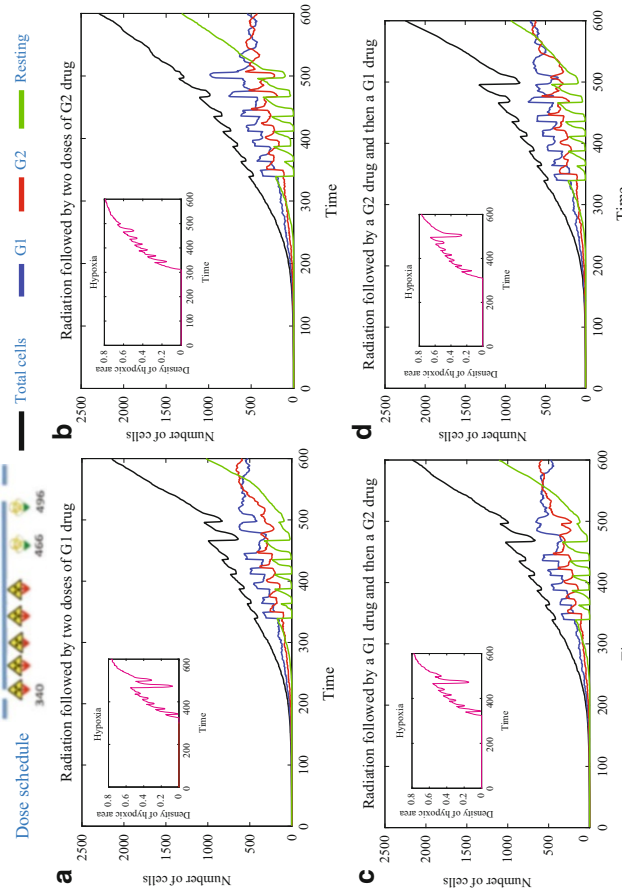

Fig. 12 Number of cells when chemotherapy is given after radiation therapy. Two doses of G1 and/or G2 drugs are given at time=466 h and 496 h, after 5 fractions of radiation therapy (1 week) with a daily dose of 2.5 Gy starting at time=340 h. (**a**) Plots when two G1-phase-specific drugs are given after radiation, (**b**) plots when two G2-phase-specific drugs are given after radiation, (**c**) plots when a G1-phase-specific drug followed by a G2 specific drug are given after radiation and (**d**) plots when a G2-phase-specific drug followed by a G2-specific drug are given after radiation. Adapted from [56]

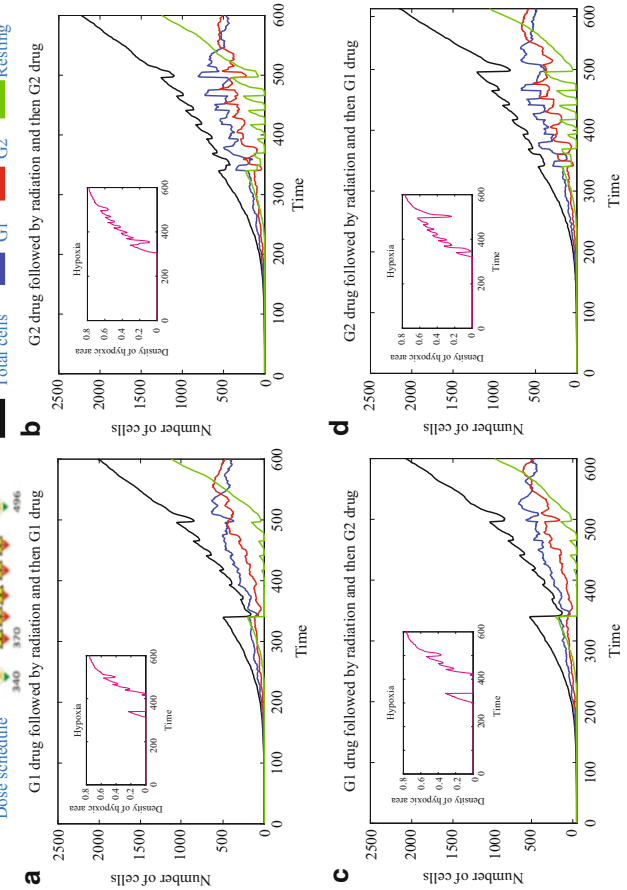

Fig. 13 Number of cells when a chemotherapy (one dose) is given before and after radiation therapy. Two doses of G1 and/or G2 drugs are given at time=340 h and 496 h and 5 fractions of radiation therapy (1 week) with a daily dose of 2.5 Gy are given in between the chemotherapy doses, starting at time=370 h. (**a**) Plots when two G1-phase-specific drugs is given, each before and after radiation, (**b**) plots when two G2-phase-specific drugs are given, each before and after radiation, (**c**) plots when a G1-phase-specific drug is given before the radiation followed by a G2-specific drug and (**d**) plots when a G2-phase-specific drug is given before radiation followed by a G2 specific drug. Adapted from [56]

favorable. Alternatively, the administration of a G2-specific drug, which kills fewer cells compared to the G1-phase-specific drug, helps to keep the cells in synchrony throughout the treatment time. However, in both cases shown, in the absence of additional fractions of radiation and further doses of chemotherapy, all the schedules perform in a similar fashion, although some give a better cell kill.

4 Conclusions

Along with the rapid growth in acquisition of genetic, proteomic and other biochemical and biological data, there has been a parallel development from the theoretical side in terms of modelling. In particular, systems biology has emerged as a field of research over the past decade applied to a wide range of problems in the biomedical sciences. Systems biology seeks to bring to bear a range of interdisciplinary skills and tools on complex biomedical problems. By adopting a holistic or integrative approach (as opposed to the more traditional reductionist logic), systems biology aims to predict emergent behavior that will arise from complex biomedical systems i.e., behavior that appears over time due to the interactions between genes, proteins, cells and tissues across a range of spatial and temporal scales. Given the complexity of most biomedical systems and the inherent nonlinearities in such systems, without adopting some kind of systems approach it is not possible to make accurate predictions. Indeed, in the last few years, systems biology itself has evolved and further developed seeking not just to understand events at the separate biological scales in a qualitative manner, but there are now mathematical models which are truly multiscale, leading to the emergence of quantitative systems biology or quantitative integrative biology. This novel systems approach is now being brought to bear on cancer modelling and a related discipline of what may be termed systems oncology now exists in its own right to develop predictive multi-scale models of cancer growth and spread.

Established mathematical models now exist for all the key phases of solid tumor growth, i.e., avascular growth [13, 14], tumor-induced angiogenesis [9, 45], the immune response to cancer [2, 43], invasion and metastasis [8, 19, 27, 58, 59] and vascular growth [41, 76]. New areas are also now being investigated concerning the spatio-temporal modelling of intracellular pathways associated with cancer such as p53-Mdmd2 [69, 70]. A comprehensive overview of the field may be found in the review article [40]. In the past few years especially, multiscale models of solid tumor growth have been developed in order to account for the different spatial and temporal scales (from genes to tissues) that occur not only in cancer but in all biological systems [3, 5, 63, 77]. A review of recent models in this area may be found in the paper of Deisboeck et al. [20]. There has also been a concerted effort to integrate mathematical models of cancer with real data in a genuine attempt to develop quantitative, predictive models [12]. Alongside these developments in the field in general, it is natural that models of cancer treatment have begun to

be formulated both for chemotherapy [1, 23, 24, 39, 46, 51, 62] and radiotherapy [22, 61, 64]. More recently models adopting a multiscale approach to treatment modelling have been developed [11].

In this chapter we have adopted a multiscale approach to modelling cancer treatment. Specifically, we have presented a hybrid multiscale cellular automaton model to study the effects of cell-cycle-phase specific chemotherapy and radiation therapy, alone and in combinations [56, 57]. The clinical and experimental observations indicated the internal and external heterogeneities within a cancer cell play important roles in prescribing the effects of chemotherapeutic drug as well as radiation therapy [53]. For this reason we incorporated the effects of cell-cycle-mediated chemotherapeutic and radiation sensitivity as well as the effects of changing oxygen and tissue dynamics within this hybrid cell-based modelling framework. The results obtained from the model are in qualitative agreement with experimental results [56] and thus show its potential usefulness in studying and understanding a kinetic administration of cell-cycle phase-specific chemotherapeutic drugs in combination with radiation therapy. Future work will consider other factors that may interfere with the cell-cycle dynamics such as circadian rhythms and wee1 dynamics and explore the therapeutic benefits of "chronotherapy," alone and in combination with the radiation therapy. Furthermore, we will also incorporate the interplay between normal cells and cancer cells, as their interactions are equally important in studying the therapeutic benefit with a minimum damage to the normal cells.

The long-term goal of such interdisciplinary, multiscale "systems oncology" modelling is to build a virtual cancer made up of different but connected mathematical models at the different biological scales (from genes to tissue to organ). The development of quantitative, predictive models (based on sound biological evidence and underpinned and parameterized by biological data) will no doubt have a positive impact on patients suffering from diseases such as cancer through improved clinical treatment and is a real motivation for becoming involved in such modelling.

Acknowledgements The authors gratefully acknowledge the support of the ERC Advanced Investigator Grant 227619, M5CGS - From Mutations to Metastases: Multiscale Mathematical Modelling of Cancer Growth and Spread.

References

1. Z. Agur, R. Hassin, S. Levy, Optimizing chemotherapy scheduling using local search heuristics. Operat. Res. **54**(5), 829–846 (2006)
2. M. Al-Tameemi, M. Chaplain, A. d'Onofrio, Evasion of tumours from the control of the immune system: consequences of brief encounters. Biol. Direct **7**, 31 (2012)
3. T. Alarcon, H.M. Byrne, P.K. Maini, A cellular automaton model for tumour growth in inhomogeneous environment. J. Theor. Biol. **225**, 257–274 (2003)
4. T. Alarcon, H.M. Byrne, P.K. Maini, A mathematical model of the effects of hypoxia on the cell-cycle of normal and cancer cells. J. Theor. Biol. **229**, 395–411 (2004)
5. T. Alarcon, H.M. Byrne,, Maini, .: A multiple scale model for tumour growth. Multiscale Model. Sim. **3**, 440–475 (2005)

6. Alper, T., Howard-Flanders, P.: Role of oxygen in modifying the radiosensitivity of E. coli B. Nature **178**(4540), 978–979 (1956)
7. A. Altinok, F. Levi, A. Goldbeter, A cell cycle automaton model for probing circadian patterns of anticancer drug delivery. Adv. Drug Deliv. Rev. **59**, 1036–1053 (2007)
8. V. Andasari, A. Gerisch, G. Lolas, A.P. South, M.A. Chaplain, Mathematical modeling of cancer cell invasion of tissue: biological insight from mathematical analysis and computational simulation. J. Math. Biol. **63**(1), 141–171 (2011)
9. A.R. Anderson, M.A. Chaplain, Continuous and discrete mathematical models of tumor-induced angiogenesis. Bull. Math. Biol. **60**, 857–899 (1998)
10. J.C. Bailar, H.L. Gornik, Cancer undefeated. N. Engl. J. Med. **336**, 1569–1574 (1997)
11. F. Billy, B. Ribba, O. Saut, H. Morre-Trouilhet, T. Colin, D. Bresch, J.P. Boissel, E. Grenier, J.P. Flandrois, A pharmacologically based multiscale mathematical model of angiogenesis and its use in investigating the efficacy of a new cancer treatment strategy. J. Theor. Biol. **260**(4), 545–562 (2009)
12. H.M. Byrne, Dissecting cancer through mathematics: from the cell to the animal model. Nat. Rev. Cancer **10**, 221–230 (2010)
13. H.M. Byrne, M.A. Chaplain, Growth of nonnecrotic tumors in the presence and absence of inhibitors. Math. Biosci. **130**(2), 151–181 (1995)
14. H.M. Byrne, M.A. Chaplain, Growth of necrotic tumors in the presence and absence of inhibitors. Math. Biosci. **135**(2), 187–216 (1996)
15. M. Chaplain, A. Anderson, Mathematical modelling of tumour-induced angiogenesis: network growth and structure. Cancer Treat. Res. **117**, 51–75 (2004)
16. M.A. Chaudhry, Base excision repair of ionizing radiation-induced DNA damage in G1 and G2 cell cycle phases. Cancer Cell. Int. **7**, 15 (2007)
17. J. Clairambault, A step toward optimization of cancer therapeutics. Physiologically based modeling of circadian control on cell proliferation. IEEE Eng. Med. Biol. Mag. **27**, 20–24 (2008)
18. A. Dasu, I. Toma-Dasu, M. Karlsson, Theoretical simulation of tumour oxygenation and results from acute and chronic hypoxia. Phys. Med. Biol. **48**, 2829–2842 (2003)
19. N.E. Deakin, M.A. Chaplain, Mathematical modeling of cancer invasion: the role of membrane-bound matrix metalloproteinases. Front. Oncol. **3**, 70 (2013)
20. T.S. Deisboeck, Z. Wang, P. Macklin, V. Cristini, Multiscale cancer modeling. Annu. Rev. Biomed. Eng. **13**, 127–155 (2011)
21. S. Dormann, A. Deutsch, Modeling of self-organized avascular tumor growth with a hybrid cellular automaton. In Silico Biol. (Gedrukt) **2**, 393–406 (2002)
22. H. Enderling, A.R. Anderson, M.A. Chaplain, A.J. Munro, J.S. Vaidya, Mathematical modelling of radiotherapy strategies for early breast cancer. J. Theor. Biol. **241**(1), 158–171 (2006)
23. K. Fister, J. Panetta, Optimal control applied to cell-cycle-specific cancer chemotherapy. SIAM J. Appl. Math. **60**, 1059–1072 (2000)
24. H.B Frieboes, M.E. Edgerton, J.P. Fruehauf, F.R. Rose, L.K. Worrall, R.A. Gatenby, M. Ferrari, V. Cristini, Prediction of drug response in breast cancer using integrative experimental/computational modeling. Cancer Res. **69**, 4484–4492 (2009)
25. K. Fu, Biological basis for the interaction of chemotherapeutic agents and radiation therapy. Cancer **55**(S9), 2123–2130 (1985)
26. C. Gerard, A. Goldbeter, Temporal self-organization of the cyclin/Cdk network driving the mammalian cell cycle. Proc. Natl. Acad. Sci. U.S.A. **106**, 21,643–21,648 (2009)
27. A. Gerisch, M.A. Chaplain, Mathematical modelling of cancer cell invasion of tissue: local and non-local models and the effect of adhesion. J. Theor. Biol. **250**(4), 684–704 (2008)
28. P. Gerlee, A.R. Anderson, An evolutionary hybrid cellular automaton model of solid tumour growth. J. Theor. Biol. **246**, 583–603 (2007)
29. N. Goda, H.E. Ryan, B. Khadivi, McNulty, W., Rickert, R.C., Johnson, R.S.: Hypoxia-inducible factor 1alpha is essential for cell cycle arrest during hypoxia. Mol. Cell. Biol. **23**, 359–369 (2003)

30. A. Goldbeter, A minimal cascade model for the mitotic oscillator involving cyclin and cdc2 kinase. Proc. Natl. Acad. Sci. U.S.A. **88**, 9107–9111 (1991)
31. M. Guerrero, X.A. Li, Analysis of a large number of clinical studies for breast cancer radiotherapy: estimation of radiobiological parameters for treatment planning. Phys. Med. Biol. **48**(20), 3307–3326 (2003)
32. S. Gupta, T. Koru-Sengul, S.M. Arnold, G.R. Devi, M. Mohiuddin, M.M. Ahmed, Low-dose fractionated radiation potentiates the effects of cisplatin independent of the hyper-radiation sensitivity in human lung cancer cells. Mol. Cancer Ther. **10**(2), 292–302 (2011)
33. C. Hennequin, V. Favaudon, Biological basis for chemo-radiotherapy interactions. European J. Cancer **38**(2), 223–230 (2002)
34. C. Hennequin, N. Giocanti, V. Favaudon, Interaction of ionizing radiation with paclitaxel (Taxol) and docetaxel (Taxotere) in HeLa and SQ20B cells. Cancer Res. **56**(8), 1842–1850 (1996)
35. A.R . Kansal, S. Torquato, G.R. Harsh IV, E.A. Chiocca, T.S. Deisboeck, Cellular automaton of idealized brain tumor growth dynamics. BioSystems **55**, 119–127 (2000)
36. M.A. Konerding, W. Malkusch, B. Klapthor, C. van Ackern, E. Fait, S.A. Hill, C. Parkins, D.J. Chaplin, M. Presta, J. Denekamp, Evidence for characteristic vascular patterns in solid tumours: quantitative studies using corrosion casts. Br. J. Cancer **80**, 724–732 (1999)
37. F. Levi, A. Okyar, Circadian clocks and drug delivery systems: impact and opportunities in chronotherapeutics. Expert Opin. Drug Deliv. **8**(12), 1535–1541 (2011)
38. F. Levi, A. Okyar, S. Dulong, P.F. Innominato, J. Clairambault, Circadian timing in cancer treatments. Annu. Rev. Pharmacol. Toxicol. **50**, 377–421 (2010)
39. W. Liu, T. Hillen, H. Freedman, A mathematical model for m-phase specific chemotherapy including the g0-phase and immunoresponse. Math. Biosci. Eng. **4**(2), 239 (2007)
40. J.S. Lowengrub, H.B. Frieboes, F. Jin, Y.L. Chuang, X. Li, P. Macklin, S.M. Wise, V. Cristini, Nonlinear modelling of cancer: bridging the gap between cells and tumours. Nonlinearity **23**, R1–R9 (2010)
41. P. Macklin, S. McDougall, A.R. Anderson, M.A. Chaplain, V. Cristini, J. Lowengrub, Multiscale modelling and nonlinear simulation of vascular tumour growth. J. Math. Biol. **58**(4–5), 765–798 (2009)
42. A. Maity, McKenna, W.G., Muschel, R.J.: The molecular basis for cell cycle delays following ionizing radiation: a review. Radiother. Oncol. **31**(1), 1–13 (1994)
43. A. Matzavinos, M.A. Chaplain, V.A. Kuznetsov, Mathematical modelling of the spatio-temporal response of cytotoxic T-lymphocytes to a solid tumour. Math. Med. Biol. **21**(1), 1–34 (2004)
44. Matzavinos, A., Kao, C.Y., Green, J.E., Sutradhar, A., Miller, M., Friedman, A.: Modeling oxygen transport in surgical tissue transfer. Proc. Natl. Acad. Sci. U.S.A. **106**, 12,091–12,096 (2009)
45. S.R. McDougall, A.R. Anderson, M.A. Chaplain, Mathematical modelling of dynamic adaptive tumour-induced angiogenesis: clinical implications and therapeutic targeting strategies. J. Theor. Biol. **241**(3), 564–589 (2006)
46. H.B. Mistry, D.E. MacCallum, R.C. Jackson, M.A. Chaplain, F.A. Davidson, Modeling the temporal evolution of the spindle assembly checkpoint and role of Aurora B kinase. Proc. Natl. Acad. Sci. U.S.A. **105**(51), 20,215–20,220 (2008)
47. B. Novak, J.J. Tyson, Modelling the controls of the eukaryotic cell cycle. Biochem. Soc. Trans. **31**, 1526–1529 (2003)
48. B. Novak, J.J. Tyson, A model for restriction point control of the mammalian cell cycle. J. Theor. Biol. **230**, 563–579 (2004)
49. M.R. Owen, T. Alarcon, P.K. Maini, H.M. Byrne, Angiogenesis and vascular remodelling in normal and cancerous tissues. J. Math. Biol. **58**, 689–721 (2009)
50. M.R. Owen, H.M. Byrne, C.E. Lewis, Mathematical modelling of the use of macrophages as vehicles for drug delivery to hypoxic tumour sites. J. Theor. Biol. **226**, 377–391 (2004)
51. J. Panetta, J. Adam, A mathematical model of cycle-specific chemotherapy. Math. Comput. Model.**22**(2), 67–82 (1995)

52. A.A. Patel, E.T. Gawlinski, S.K. Lemieux, R.A. Gatenby, A cellular automaton model of early tumor growth and invasion. J. Theor. Biol. **213**, 315–331 (2001)
53. Pawlik, T.M., Keyomarsi, K.: Role of cell cycle in mediating sensitivity to radiotherapy. Int. J. Radiat. Oncol. Biol. Phys. **59**(4), 928–942 (2004)
54. Perfahl, H., Byrne, H.M., Chen, T., Estrella, V., Alarcon, T., Lapin, A., Gatenby, R.A., Gillies, R.J., Lloyd, M.C., Maini, P.K., Reuss, M., Owen, M.R.: Multiscale modelling of vascular tumour growth in 3D: the roles of domain size and boundary conditions. PLoS ONE **6**, e14,790 (2011)
55. G. Powathil, M. Kohandel, M. Milosevic, S. Sivaloganathan, Modeling the spatial distribution of chronic tumor hypoxia: implications for experimental and clinical studies. Comput. Math. Meth. Med. **2012**, 410,602 (2012)
56. G.G. Powathil, D.J.A. Adamson, M.A.J. Chaplain, Towards predicting the response of a solid tumour to chemotherapy and radiotherapy treatments: Clinical insights from a computational model. PLOS Computational Biology (To appear) (2013). DOI 10.1371/journal.pcbi.1003120
57. G.G. Powathil, K.E. Gordon, L.A., Hill, M.A. Chaplain, Modelling the effects of cell-cycle heterogeneity on the response of a solid tumour to chemotherapy: Biological insights from a hybrid multiscale cellular automaton model. J. Theor. Biol. **308**, 1–9 (2012)
58. I. Ramis-Conde, M.A. Chaplain, A.R. Anderson, D. Drasdo, Multi-scale modelling of cancer cell intravasation: the role of cadherins in metastasis. Phys. Biol. **6**(1), 016,008 (2009)
59. I. Ramis-Conde, D. Drasdo, A.R. Anderson, M.A. Chaplain, Modeling the influence of the E-cadherin-beta-catenin pathway in cancer cell invasion: a multiscale approach. Biophys. J. **95**(1), 155–165 (2008)
60. B. Ribba, T. Alarcon, K. Marron, P. Maini, Z. Agur, The Use of Hybrid Cellular Automaton Models for Improving Cancer Therapy. Lect. Notes Comput. Sci **3305**, 444–453 (2004)
61. B. Ribba, T. Colin, S. Schnell, A multiscale mathematical model of cancer, and its use in analyzing irradiation therapies. Theor. Biol. Med. Model. **3**, 7 (2006)
62. B. Ribba, K. Marron, Z. Agur, T. Alarcon, P.K. Maini, A mathematical model of Doxorubicin treatment efficacy for non-Hodgkin's lymphoma: investigation of the current protocol through theoretical modelling results. Bull. Math. Biol. **67**(1), 79–99 (2005)
63. B. Ribba, O. Saut, T. Colin, D. Bresch, E. Grenier, J.P. Boissel, A multiscale mathematical model of avascular tumor growth to investigate the therapeutic benefit of anti-invasive agents. J. Theor. Biol. **243**(4), 532–541 (2006)
64. M. Richard, K. Kirkby, R. Webb, N. Kirkby, A mathematical model of response of cells to radiation. Nuclear Instruments and Meth. Phy. Res. Section B: Beam Interactions Mater. Atoms **255**(1), 18–22 (2007)
65. R.K. Sachs, P. Hahnfeld, D.J. Brenner, The link between low-LET dose-response relations and the underlying kinetics of damage production/repair/misrepair. Int. J. Radiat. Biol. **72**(4), 351–374 (1997)
66. G.K. Schwartz, M.A. Shah, Targeting the cell cycle: a new approach to cancer therapy. J. Clin. Oncol. **23**, 9408–9421 (2005)
67. G. Serini, D. Ambrosi, E. Giraudo, A. Gamba, L. Preziosi, F. Bussolino, Modeling the early stages of vascular network assembly. EMBO J. **22**, 1771–1779 (2003)
68. E. Shochat, D. Hart, Z. Agur, Using computer simulations for evaluating the efficacy of breast cancer chemotherapy protocols. Math. Models Meth. Appl. Sci. **9**(4), 599–615 (1999)
69. M. Sturrock, A.J. Terry, D.P. Xirodimas, A.M. Thompson, M.A. Chaplain, Spatio-temporal modelling of the Hes1 and p53-Mdm2 intracellular signalling pathways. J. Theor. Biol. **273**(1), 15–31 (2011)
70. M. Sturrock, A.J. Terry, D.P. Xirodimas, A.M. Thompson, M.A. Chaplain, Influence of the nuclear membrane, active transport, and cell shape on the Hes1 and p53-Mdm2 pathways: insights from spatio-temporal modelling. Bull. Math. Biol. **74**(7), 1531–1579 (2012)
71. I.Tannock, R. Hill, R. Bristow, L. Harrington, *Basic Science of Oncology* (MacGraw Hill, Boston 2005)
72. I. Turesson, J. Carlsson, A. Brahme, B. Glimelius, B. Zackrisson, B. Stenerlow, Biological response to radiation therapy. Acta Oncol **42**(2), 92–106 (2003)

73. S. Turner, J.A. Sherratt, Intercellular adhesion and cancer invasion: a discrete simulation using the extended Potts model. J. Theor. Biol. **216**, 85–100 (2002)
74. J.J. Tyson, B. Novak, Regulation of the eukaryotic cell cycle: molecular antagonism, hysteresis, and irreversible transitions. J. Theor. Biol. **210**, 249–263 (2001)
75. B.G. Wouters, J.M. Brown, Cells at intermediate oxygen levels can be more important than the "hypoxic fraction" in determining tumor response to fractionated radiotherapy. Radiat. Res. **147**(5), 541–550 (1997)
76. M. Wu, H.B. Frieboes, S.R. McDougall, M.A. Chaplain, V.Cristini, J. Lowengrub, The effect of interstitial pressure on tumor growth: coupling with the blood and lymphatic vascular systems. J. Theor. Biol. **320**, 131–151 (2013)
77. L. Zhang, Z. Wang, J.A. Sagotsky, T.S. Deisboeck, Multiscale agent-based cancer modeling. J. Math. Biol. **58**(4–5), 545–559 (2009)